Green Chemistry

PAPER

Cite this: *Green Chem.*, 2021, **23**, 1748

NO_x production in a rotating gliding arc plasma: potential avenue for sustainable nitrogen fixation†

Fatme Jardali, *‡[a] Senne Van Alphen, ‡[a,b] James Creel, [a] Hamid Ahmadi Eshtehardi, [a,c] Magnus Axelsson,[d] Rune Ingels,[d] Rony Snyders[b] and Annemie Bogaerts *[a]

Received 18th October 2020,
Accepted 27th January 2021

DOI: 10.1039/d0gc03521a

rsc.li/greenchem

The fast growing world population demands food to survive, and nitrogen-based fertilizers are essential to ensure sufficient food production. Today, fertilizers are mainly produced from non-sustainable fossil fuels *via* the Haber–Bosch process, leading to serious environmental problems. We propose here a novel rotating gliding arc plasma, operating in air, for direct NO_x production, which can yield high nitrogen content organic fertilizers without pollution associated with ammonia emission. We explored the efficiency of NO_x production in a wide range of feed gas ratios, and for two arc modes: rotating and steady. When the arc is in steady mode, record-value NO_x concentrations up to 5.5% are achieved which are 1.7 times higher than the maximum concentration obtained by the rotating arc mode, and with an energy consumption of 2.5 MJ mol^{-1} (or *ca.* 50 kW h kN^{-1}); *i.e.* the lowest value so far achieved by atmospheric pressure plasma reactors. Computer modelling, using a combination of five different complementary approaches, provides a comprehensive picture of NO_x formation in both arc modes; in particular, the higher NO_x production in the steady arc mode is due to the combined thermal and vibrationally-promoted Zeldovich mechanisms.

Introduction

All living organisms on earth require nitrogen (N) to survive because it is one of the six essential building blocks for life. In its molecular form, however, nitrogen (N_2) remains unusable by humans and other species, despite its high content in the atmosphere, because of its stability and inertness. Therefore, its transformation or fixation into reactive nitrogen (Nr) compounds, such as ammonia (NH_3), ammonium (NH_4^+), nitric oxide (NO), nitrogen dioxide (NO_2), nitric acid (HNO_3) and nitrate (NO_3^-), is crucial to maintain and increase the production of food in order to feed the global human population, which will reach nearly ten billion by 2050.[1]

Livestock waste contains considerable quantities of Nr, but approximately 50% of the nutrients in the manure are lost as emissions in the form of volatile NH_3, created when bacteria degrade the waste, and in the form of nitrous oxide (N_2O), a major greenhouse gas (GHG). Such losses dramatically decrease the N-fertilizer value of organic waste and contribute to pollution problems that cause severe damage to human health and ecosystem services.[2] In current agricultural practices, these lost nutrients are replaced by synthetic chemical fertilizers. At present, NH_3 is manufactured *via* the industrial Haber–Bosch (HB) process by reacting N_2 and H_2 in the presence of a catalyst at high pressures and temperatures.[3] HB plants equipped with the most advanced available technologies consume about 0.5 MJ per mole of NH_3 produced (0.5 MJ mol^{-1} NH_3), an energy consumption value close to the thermodynamic minimum energy of 0.3 MJ mol^{-1}.[4,5] The HB process is certainly one of the most impactful inventions as it increased the agricultural yield and was responsible for feeding about 50% of the world population as of 2008.[6] However, it is a fossil-based chemical synthesis process that consumes 1–2% of the world's total energy production, accounts for 3–5% of the worldwide natural gas consumption for the production of H_2, and consequently, generates about 1.9 metric tons of carbon dioxide (CO_2) per metric ton of NH_3 produced.[6] In this sense, a minor optimisation in the nitrogen

[a]*Research group PLASMANT, Department of Chemistry, University of Antwerp, Universiteitsplein 1, BE-2610 Antwerp, Belgium. E-mail: fatme.jardali@uantwerpen.be, annemie.bogaerts@uantwerpen.be*
[b]*Research group ChIPS, Department of Chemistry, University of Mons, Av. Nicolas Copernic 3, 7000 Mons, Belgium*
[c]*4MAT, CP 165/63, Université Libre de Bruxelles, 50 Av. F.D. Roosevelt, B-1050 Brussels, Belgium*
[d]*N2Applied, Beddingen 2, NO-0250 Oslo, Norway*
†Electronic supplementary information (ESI) available. See DOI: 10.1039/d0gc03521a
‡Shared first author.

fixation process multiplied by the world-scale production could result in huge economic and environmental savings.

Minimizing or eliminating NH_3 losses in livestock manure is an essential step towards increasing the efficiency of nitrogen utilization and reducing human perturbation to the global nitrogen cycle. This can be achieved by converting volatile NH_3 into involatile ammonium nitrate (NH_4NO_3) by treating the manure with HNO_3 (see ESI, section S.1,† for a description of the chemical reactions). HNO_3 can be easily formed by dissolving NO_2 in water *via* the reaction $3NO_2 + H_2O \rightarrow 2HNO_3 + NO$. After waiting for a long time during the absorption process, the formed NO will react with O_2 and H_2O to form HNO_3 according to $4NO + 3O_2 + 2H_2O \rightarrow 4HNO_3$.

Using an electrically-driven plasma source, N_2 and O_2 from air can be transformed into reactive NO and NO_2 (*i.e.* NO_x),[7] which can then be mixed with livestock manure on site to form the nitrate that stabilizes the ammonium.[8] The resulting NH_4NO_3 compound and the changes in pH of this composition enhance the nitrogen value of the organic fertilizer and prevent GHG emissions to the atmosphere. Such a combined technology is able to recycle nature's nitrogen, eliminate pollution and create an economic benefit for farmers.[8] Needless to say, it can be complementary to the HB process and not necessarily a direct competitor.

Plasma is an ionized gas, created in its simplest form by applying electricity to a gas, causing gas breakdown, and the formation of many reactive species, *i.e.*, electrons, ions, radicals, excited species, besides neutral molecules. The use of plasma technology is picking up across various sectors due to its potential benefits, for example, for the conversion of CO_2 and methane (CH_4) into value-added chemicals or renewable fuels.[9,10] Plasma offers several advantages, as it enables thermodynamically unfavourable chemical reactions at ambient conditions due to its reactive environment, and it can be ignited and shut off instantaneously showing that it is very attractive in combination with fluctuating renewable electricity, for peak shaving and grid stabilization.[7] Therefore, the conversion of abundant air into valuable products in a plasma reactor can be accomplished using renewable energy sources.

The first industrial application of a thermal plasma for nitrogen fixation is the electric arc process developed by Birkeland and Eyde in Norway in 1903.[11,12] In their process, air flows through an arc discharge zone, producing about 2% NO. Due to its higher energy cost (2.0–3.28 MJ mol^{-1}) compared to the original HB process (1.4 MJ mol^{-1}), the air plasma process was rebuilt, in order to use electricity for the production of hydrogen from water and nitrogen from air and convert it to ammonia through the HB process.[6]

Quite some research has been dedicated already to NO_x synthesis using different types of plasma sources.[13–28] The reported NO_x concentrations and energy consumptions for different plasma types are summarized in Table S1 in ESI, section S.2.† To date, the lowest energy consumption (0.28 MJ mol^{-1}) and highest NO_x concentration (14%) have been achieved with a microwave (MW) plasma together with a magnetic field.[19] However, these values were obtained in 1980 and have never been reproduced since then. Furthermore, this MW reactor was operated at reduced pressure (down to 66 mbar), and the reported energy cost accounts for the plasma power only and does not include the energy consumed by both the vacuum equipment and the reactor cooling system. Therefore, the total energy cost of this MW system would end up at a considerably higher value, making this technology less appealing for industrial purposes. Several studies have been dedicated to explore the efficiency of different atmospheric-pressure plasma types[15,16,20,25–28] (see Table S1 in ESI†). Gliding arc (GA) plasmas have shown the most promising results:[15,16,28] up to 2% in NO_x concentration and down to 2.8 MJ mol^{-1} in energy cost.

However, major efforts are still needed for air plasma technology to become commercially attractive. In the present study, we explore the efficiency of a novel atmospheric pressure gliding arc plasma reactor, so-called rotating gliding arc (RGA), for producing NO and NO_2 by means of a combined experimental and computational study. We measured NO_x concentrations for a wide range of N_2/O_2 feed ratios, and for an arc operating in two different modes: a rotating arc with variable length and a steady arc with stable length. We thoroughly investigated the behaviour of the arc and the underlying chemistry in both modes by means of fluid dynamics and chemical kinetics modelling, providing a comprehensive picture on NO_x formation in the RGA.

Description of the experiments

Fig. 1(a) shows the experimental setup of our RGA plasma reactor and Fig. 1(b) illustrates the reactor configuration. The plasma reactor consists of two electrodes: an internal nickel electrode (cathode) to which the high voltage is applied, and a grounded stainless-steel electrode (anode) acting as reactor body (see Fig. 1(b)). Essentially, a spark plug (NGK BP6ES) is used as the powered electrode (with its ground pin being removed and replaced by the stainless steel RGA body). The reactor body has a cone shape with largest diameter of 13 mm and extends to the outlet in a cylindrical shape with diameter of 4 mm. The length of the reactor body is 38.2 mm. A ceramic electric insulator separates both electrodes with shortest gap of 4 mm. An additional stainless-steel cylinder is added to the reactor body to confine the exhaust gas and to provide connection to the gas analysis instrument. The arc discharge is generated by a 10 kV DC power supply (Topower TN-XXZ02). A 25 kΩ ballast resistor is connected to the circuit to compensate for changes in the discharge current and to prevent over-heating of the plasma, allowing for a maximum current of 280 mA. The discharge voltage is measured by a high-voltage probe (TESTEC 1000 : 1), and the discharge current is determined from the voltage drop across a 25 Ω resistor. The time-resolved waveforms of the discharge voltage and current are recorded by an oscilloscope (Keysight DSOX1102A, 70 MHz bandwidth, 2 GSa s^{-1} sample rate).

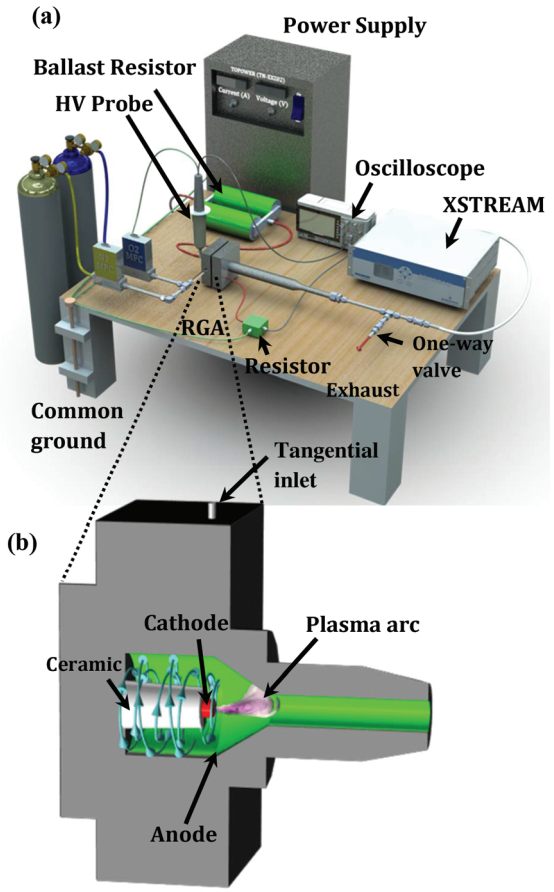

Fig. 1 Experimental setup used for NO_x production (a) and configuration of the RGA plasma reactor showing some gas velocity streamlines and the plasma arc (b). XSTREAM detector image courtesy Emerson.com.

The discharge power (P) is calculated by:

$$P[W] = \sum_{j=1}^{N} \frac{V_j I_j}{N} \quad (1)$$

V_j and I_j are the recorded plasma voltage and current, respectively, and N is the number of records.

N_2 and O_2 feed gases (99.999% in purity) are mixed and injected into the reactor through a tangential inlet with a diameter of 1 mm, forming a swirling flow (see Fig. 1(b)). The gas flow rates are controlled by mass flow controllers (Bronkhorst model F-201CV). The total flow rate is fixed at 2 L min^{-1}, and the gas feed ratio between N_2 and O_2 is varied from 0.25 to 4.

We only focus on the total NO_x (*i.e.*, sum of NO and NO_2) concentration, as explained in the ESI (sections S.3 and S.4†). Using the power and the total NO_x concentration (c_{NOx}), we calculate the energy cost of NO_x formation as:

$$\text{Energy cost}\,[\text{MJ mol}^{-1}] = \frac{P[J\,s^{-1}] \times 24\,[L\,mol^{-1}] \times 60\,[s\,\text{min}^{-1}] \times 100[\%]}{c_{NO_x}[\%] \times Q\,[L\,\text{min}^{-1}]} \times 10^{-6}. \quad (2)$$

The value of 24 L mol^{-1} is the molar volume of ideal gas at the reactor inlet (1 atm and 293 K), Q is the total gas flow rate and 10^{-6} is the conversion factor from J to MJ.

The exhaust gas (comprising the product and unconverted feed gas) is analysed using a non-dispersive infra-red sensor along with an ultra-violet sensor for quantitative analysis of the species concentration (EMERSON-Rosemount X-STREAM Enhanced XEGP continuous Gas Analyzer) (see ESI, section S.3† for more details). The experiments are performed three times for each condition on different days and the average is taken over a 10-minute measurement period. The reported values and error bars are the weighted average of those values from different measurements.

Description of the models

A combination of five different complementary modelling approaches, including gas flow, 3D thermal plasma, 2D non-thermal plasma, chemical kinetics modelling and particle tracing simulations, are performed in order to provide a comprehensive picture on NO_x formation in the RGA. More details can be found in the ESI† and in ref. 29.

Gas flow model

The behaviour of the gas flow in the reactor is simulated by a turbulent gas flow model, so-called Reynolds-Averaged-Navier-Stokes (RANS) turbulent model, within COMSOL Multiphysics®.[30] The Navier-Stokes equations are solved for the mass and momentum conservation, and the turbulence is described by the Menter's Shear Stress Transport (SST) model. The turbulent flow model is solved independently from the other four models, *i.e.*, we assume that the flow in the reactor is not influenced by the heat produced by the plasma or by changes in gas composition due to chemical reactions. This assumption is valid as any influences from gas heating are small in comparison to the strong background inflow from the inlet, while the chemical conversion is too limited (*i.e.* % range) to significantly change the physical properties of the flow. A detailed description of the gas flow model is given in the ESI (section S.5†).

3D thermal plasma model

In order to simulate the plasma arc in the reactor, an electric circuit is added to the turbulent gas flow simulations using the "electric circuit and electric currents" module in COMSOL Multiphysics®. This is done by connecting a voltage source of 2–3 kV to the cathode while keeping the reactor walls grounded. The gas breakdown and arc formation between the cathode and the anode walls are simulated by solving a current conservation equation based on Ohm's law, using the electric potential and the electric conductivity as dependent variables. More information about the electric circuit of the model is given in the ESI (section S.6†). Additionally, this model calculates the increase in gas temperature and the corresponding increase in electric conductivity as the electric current flows

through the gas between both electrodes. The gas temperature is calculated by the gas thermal balance equation. Description of the equations solved in this model is given in the ESI (section S.7†). The temperature dependency of the electric conductivity is given by an interpolation table in the ESI (Table S.5 in section S.8†).

2D non-thermal plasma model

The thermal plasma model can correctly describe the gas temperature gradients and the three-dimensional movement of the arc. However, it assumes that the plasma is in thermal equilibrium, *i.e.*, the temperature of the gas molecules and electrons is equal. GA plasmas, however, are known to be "quasi-thermal" or "warm" plasmas, *i.e.*, the applied electrical energy predominantly heats the light electrons, resulting in thermal non-equilibrium between the electrons and gas molecules.[31,32] As a result, the gas temperature calculated by the thermal model is too high and needs to be corrected. This is accomplished by using a more comprehensive non-thermal plasma model that describes the individual behaviour of all plasma species (*i.e.*, electrons, various ions, radicals, molecules and excited species). This model balances the diffusion, convection and migration of all plasma species with their production or loss rates due to chemical reactions, while simultaneously calculating the gas temperature and electric field in the reactor. However, a 3D non-thermal plasma model, including all the transport terms for all species and all chemical reactions, would require excessive computation times. Therefore, we developed a 2D axisymmetric and quasi-neutral plasma model with limited reaction set; see details in the ESI (section S.9†). This approach was used for modelling the plasma arc in other types of GA reactors for gas conversion applications and provided very satisfying results.[33–35] Since the 2D non-thermal plasma model correctly incorporates the heat terms of all plasma processes and chemical reactions in the N_2/O_2 plasma, its results can be used to correct for the gas temperatures obtained by the 3D thermal plasma model, as explained in the ESI (section S.10†).

Therefore, we assume that the temperature calculated in a 2D axisymmetric non-thermal plasma model can be used as a reference to assess the temperature in an arc moving in three dimensions. This assumption is based on the fact that the magnitude of the main heat source, *i.e.*, the exothermic plasma reactions, remains the same in an axial symmetric reactor geometry.

Quasi-1D plasma chemical kinetics model

A chemical kinetics model is developed to calculate the NO_x concentration and to reveal the chemical pathways for NO_x formation in the plasma reactor. The Zero-Dimensional Plasma Kinetics solver, ZDPlasKin,[36] is used to calculate the species number densities by solving the continuity equations for all species, taking into account the production and loss terms by the chemical reactions. Details about the equation and the chemistry set are given in the ESI (sections S.11–S.13†). Transport processes are not considered, *i.e.*, the species densities are assumed to be constant in the entire simulation volume, allowing for the incorporation of an extensive plasma chemistry set. However, spatial variations are incorporated by translating the temporal behaviour of the (batch) model into a spatial behaviour (plug flow reactor model), by means of the gas velocity, yielding a quasi-1D model. In order to account for the spatial variations and to properly describe the plasma conditions that the species experience at different locations in the reactor, results obtained from the 3D models, such as gas temperature and power density profiles, are used as input for the chemical kinetics model. This is done by performing particle tracing simulations as explained below. Therefore, quasi-1D simulations are performed along the flow lines of the particles in the tracing simulation, which only considers the convection of the chemical species through the flow while neglecting any transport through diffusion (and migration for charged particles). Due to the high velocity in the vortex flow of the reactor, convection is the most significant mode of transport for all chemical species, justifying this assumption.

Particle tracing simulations

Particle tracing simulations serve as a bridge between the higher dimensional models and the chemical kinetics model. This model computes the trajectories of gas molecules and reports the conditions they experience as a function of time, as they flow through the plasma to the reactor outlet. The particle trajectories are calculated using the "particle tracing" module in COMSOL Multiphysics®, based on the drag force and velocity fields that were previously computed by the turbulent flow model; see details in the ESI (section S.14†). The trajectory calculations are performed for 10 000 particles, resulting in 10 000 possible trajectories the gas molecules can take and, hence, the different conditions (*e.g.*, temperature, power density, *etc.*) that the particles can experience throughout their trajectories. Because several of the calculated trajectories coincide, trajectories that experience a similar gas temperature are averaged together. By applying such a grouping, particles are distributed into a distinct number of groups, each described by the specific plasma conditions they experience in the reactor. Subsequently, a quasi-1D chemical kinetics simulation is performed for each group (using the plasma conditions experienced by this group) and the NO_x concentration is calculated for each group. Finally, the overall NO_x concentration is calculated from a weighted average of the concentrations obtained from the different simulations.

Results and discussion

Two distinct operation modes of the plasma arc

Our RGA reactor can operate in two distinct modes, depending on the applied power: a rotating arc with variable length (Mode I) and a more or less steady arc with stable length (Mode II).

When a voltage of about 3 kV is supplied to the reactor, the gas breaks down and a plasma is ignited, *i.e.*, an arc forms in

the shortest gap between cathode and anode. Immediately, the arc starts gliding along the reactor body with the swirling gas flow: one side of the arc remains attached to the top face of the cathode, while the other side glides around the surface of the reactor body (anode) (see Fig. 1(b)), resulting in arc elongation. While the arc is gliding, it also rotates around the internal surface of the anode. The elongation of the arc is represented by the nearly linear increase in the discharge voltage, as shown in Fig. 2(a). The discharge current decreases due to the rising arc length, and thus rising arc resistance. During arc elongation, energy is dissipated. Therefore, if the supplied power is not sufficient to sustain further arc extension (*i.e.*, up to about 110 W), the arc will extinguish (represented by a sudden drop of the discharge voltage in Fig. 2(a)), and re-ignition will take place in the shortest gap between both electrodes. Extinguishing and re-ignition of the arc continues to occur in Mode I. This is the common operating mode of the RGA reactor. In Mode II, however, the supplied power is above 180 W, which is high enough for the arc to elongate and reach the furthest point of contact on the reactor outlet. At this high power, the arc does not extinguish, and remains relatively stable in the centre of the reactor with a constant arc length, which is also reflected by the current–voltage characteristics in Fig. 2(b), showing constant values over time.

NO_x concentration produced and corresponding energy cost

Fig. 3 displays the NO_x concentrations and corresponding energy cost, for the plasma arc in Mode I (a and c) and Mode II (b and d), as a function of the N_2/O_2 feed ratio, obtained in the experiments, and compared with the calculation results of the combined models. The NO_x concentration is calculated for each group of particles by a quasi-1D chemical kinetics simulation (using the plasma conditions experienced by each group). Finally, the overall NO_x concentration is calculated as the weighted average of the concentrations obtained from the different simulations for each group. Note that the measured and calculated energy costs are both plotted using the same axes, and the values are given both in MJ mol^{-1} and kW h kN^{-1}, for easy comparison with literature, where energy cost is sometimes given in either unit.

The operating current is 70 mA for Mode I, and varies between 115 and 149 mA, depending on the gas composition, for Mode II. In Mode I, the 40% N_2/60% O_2 mixture provides the highest NO_x concentration of 3.4% and the lowest energy cost of 2.4 MJ mol^{-1} (see Fig. 3(a and c)). The modelling results are in reasonable agreement with the experiments, showing a similar trend in both the NO_x concentration and energy cost as a function of gas feed ratio. At a gas composition close to the composition of air, *i.e.* 80% N_2/20% O_2, we find a slight drop in the NO_x concentration, down to 2.5%, and a consequent rise in the energy cost, up to 3.0 MJ mol^{-1}. The reason is that at a higher N_2 content, more energy is required to break the very strong triple bond of N_2, and not enough O_2 is present which is equally needed for NO_x formation. Nevertheless, compared to other atmospheric pressure plasma reactors (see Table S1 in the ESI†), the RGA operating in Mode I generally already provides better NO_x concentrations with lower energy consumption.

Interestingly, when operating the plasma reactor in Mode II, we find a further increase in the NO_x concentration, reaching up to 5.5% for a 50% N_2/50% O_2 gas mixture, *i.e.*, 1.7 times more than the maximum concentration achieved in Mode I. Such a high NO_x concentration has never been obtained in any plasma reactor operating at atmospheric pressure (see Table S1 in the ESI†). Again, good agreement is obtained with the modelling results (see Fig. 3(b)). The high NO_x concentrations formed, in combination with the plasma powers used in this mode (between 180 and 200 W) result in an energy consumption of 2.6–2.8 MJ mol^{-1} (or *ca.* 52–56 kW h kN^{-1}) for two gas compositions (*i.e.*, 40/60 and 50/50 N_2/O_2). Again, at higher N_2 contents, the NO_x concentration in Mode II drops to 4.1% with an energy cost of 3.1 MJ mol^{-1} (see Fig. 3 (b and d)).

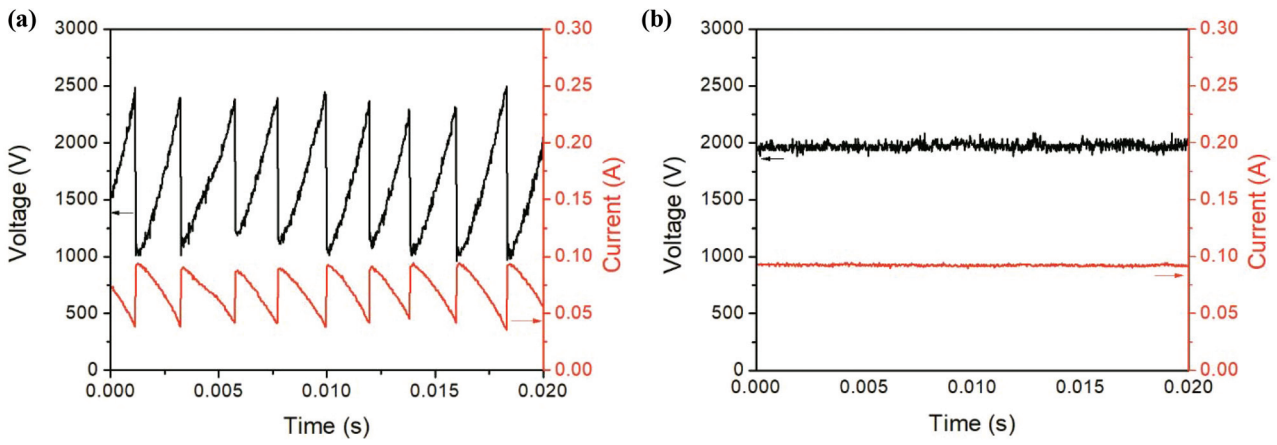

Fig. 2 Current–voltage characteristics of the plasma arc in Mode I (a) and Mode II (b), for a 50% N_2/50% O_2 gas composition. The average plasma power for Modes I and II are 108 and 200 W, respectively.

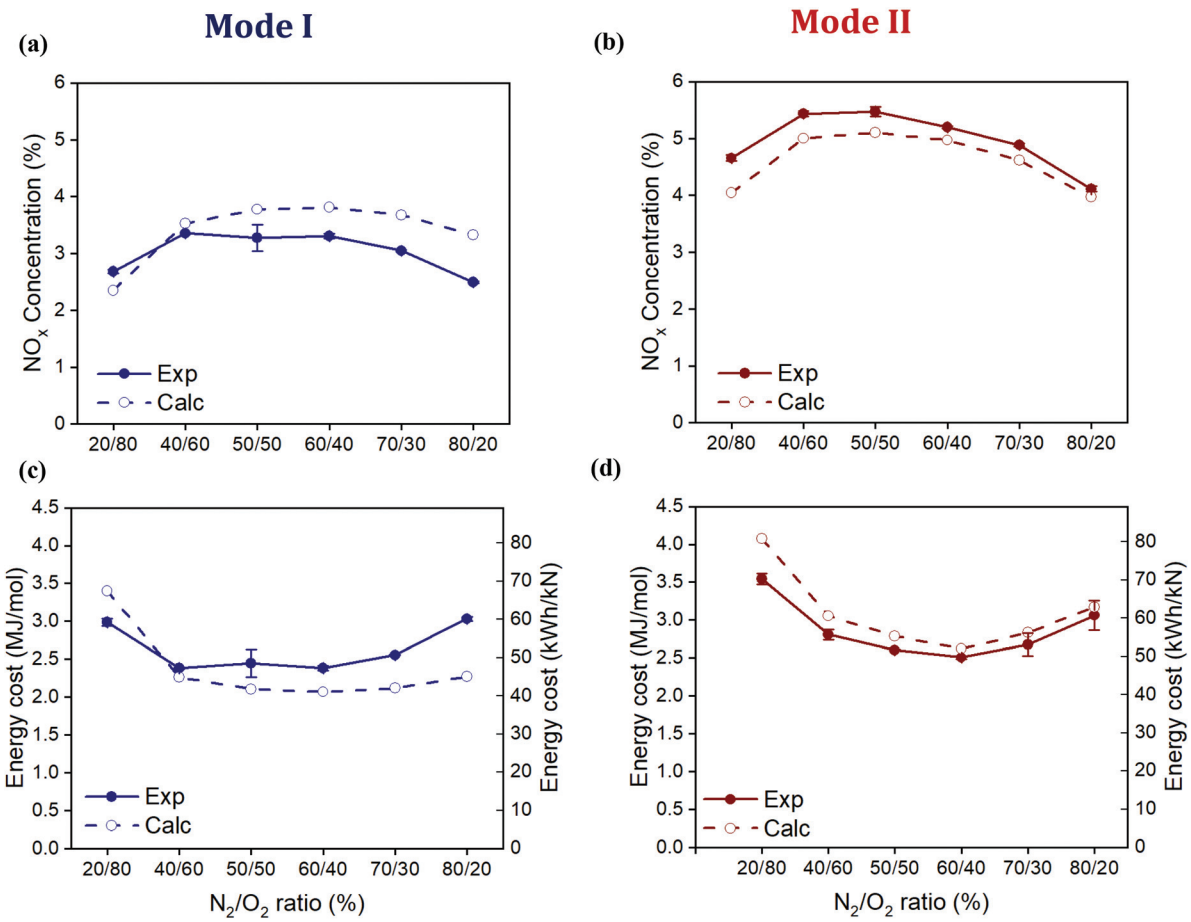

Fig. 3 Experimental and calculated NO_x concentrations in Mode I (a) and Mode II (b), and corresponding energy cost of NO_x production (c) and (d), as a function of the N_2/O_2 feed ratio. The error bars in the experimental data are obtained from the standard deviation of the measurements, and they are sometimes too small to be visible.

Understanding the different performances of both arc operating modes

As the calculation results are in reasonable agreement with the experimental data, both in absolute values and in trends, we can use our models for a deeper understanding of the different performances of both arc modes. A combination of the higher dimensional models yields information on the plasma arc movement, the trajectory of the gas molecules along the reactor, and the plasma conditions they experience throughout their path.

Mode I. Fig. 4(a) displays the calculated gas temperature at different time instants during the rotation of the arc, using a combination of the 3D thermal and 2D non-thermal plasma models (see model description). The vortex gas flow drags and rotates the plasma arc along the reactor walls. This rotational movement results in cycles of very fast gas heating and cooling, *i.e.*, every arc rotation the gas heats up to 2850 K, then cools down to about 500 K and heats again back to 2850 K (see Fig. 4(b)). Such a fast gas heating and cooling has a significant effect on the plasma chemistry. As reported by Wang *et al.*[15] and Vervloessem *et al.*,[16] the plasma chemistry in GA reactors is greatly influenced by the vibrational excitation of N_2 and O_2 molecules. In the RGA reactor, the reduced electric field is in the range of 5–30 Td, and therefore about 90% of the electron energy is transferred to vibrational excitation of N_2 molecules in a 80%N_2/20% O_2 gas mixture; see ESI (Fig. S3, section S.15†). This vibrational excitation facilitates the splitting of the strong triple bond of the N_2 molecule (≈10 eV) and promotes NO_x production through the Zeldovich mechanism:

$$O + N_2(V) \rightarrow N + NO, \quad (1)$$

followed by

$$N + O_2(V) \rightarrow O + NO. \quad (2)$$

Note that the further NO to NO_2 conversion proceeds by:

$$NO + O \rightarrow NO_2 \quad (3)$$

However, when the gas temperature is close to 3000 K, as for example in typical GA plasma reactors, the lifetime of these vibrationally excited molecules becomes shorter than a millisecond, because the high gas temperature greatly increases the rate of vibrational-translational (VT) relaxation. Hence,

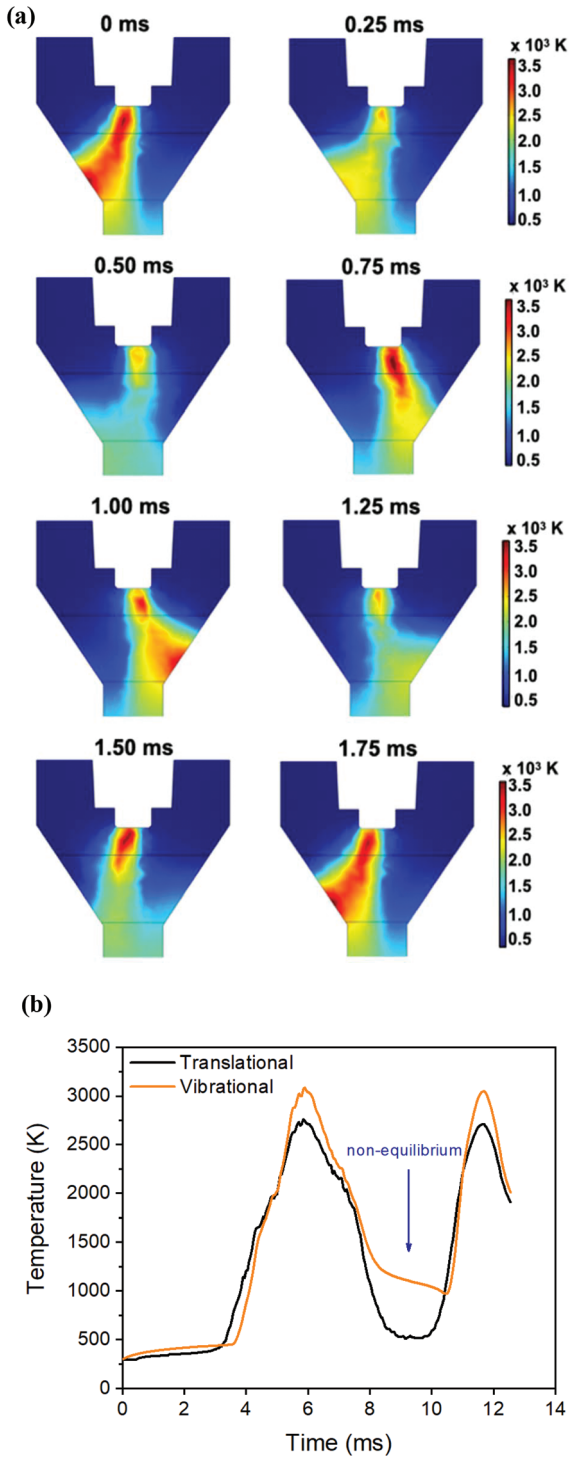

Fig. 4 Calculated plasma gas temperature at different time instants during the rotation of the plasma arc in Mode I (a), and time evolution of the translational and vibrational temperature of the N_2 molecules (b). When the molecules encounter the arc, the translational and vibrational temperature are nearly equal, but in between two arc rotations, there is VT non-equilibrium.

depopulating the vibrational levels, and resulting in gas translational and vibrational temperatures that are nearly equal (VT equilibrium).[16] In this rotational mode, however, the fast cooling prevents these relaxation processes from taking place, allowing for the vibrationally excited molecules to survive significantly longer (typical lifetime of around one second). As shown by the time evolution of the N_2 translational and vibrational temperatures for gas molecules experiencing two full arc rotations in Fig. 4(b), a non-equilibrium exists between both temperatures during the time the molecules do not pass through the arc (because of rotation of the latter), due to the very fast cooling of the gas, inhibiting the relaxation of the vibrationally excited molecules. Because of the relatively long lifetime of the vibrationally excited molecules (see above) in this rotating arc mode, more than 99% of NO_x is formed through the vibrationally-promoted Zeldovich mechanism (reactions (1)–(2) above), as revealed by our model.

Fig. 5(a) illustrates the gas temperature that the gas molecules experience while flowing through the reactor, according to our particle tracing simulations. The temperature intervals of the groups are chosen to be smaller in the range between 2000 K and 3200 K where the gas conversion is mostly sensitive

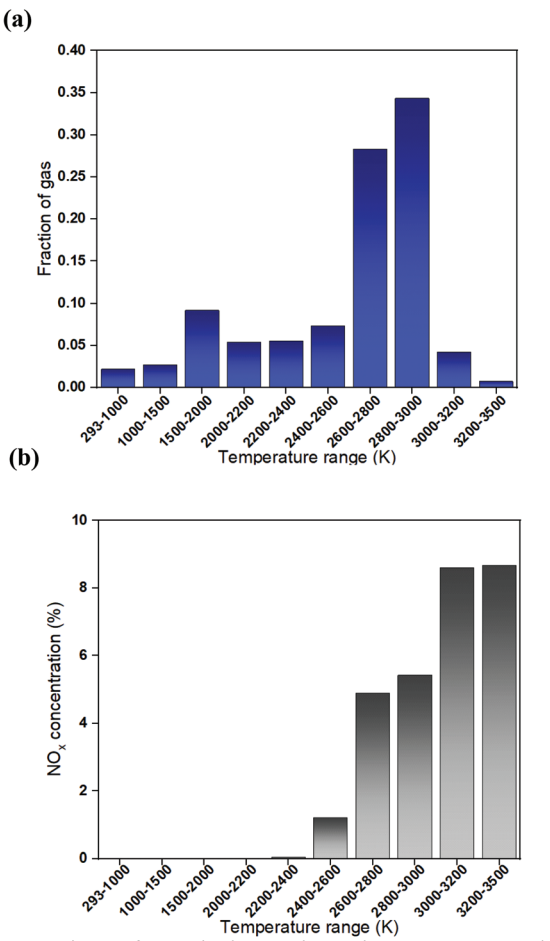

Fig. 5 Distribution of gas molecules according to the temperature range the gas molecules experience while flowing through the reactor (a), and calculated NO_x concentration obtained for each group of molecules (temperature range) (b), for a gas mixture of 50% N_2 and 50% O_2, in Mode I.

to the temperature. Around 15% of the gas molecules flow through the reactor where the gas temperature is below 2000 K and thus might not be converted. This amount of untreated gas is, however, significantly less than in other GA designs, such as a classical (2D) GA reactor[15] or the so-called gliding arc plasmatron (GAP),[16] where 85% of the gas flows through the reactor without actually passing through the arc plasma. This explains the higher NO_x production in the RGA compared to the GAP (see Table S1 in ESI†). Most of the gas molecules (60%) experience a temperature between 2600 K and 3000 K, *i.e.*, the hot zone located in the centre of the plasma arc.

Our model also reveals the NO_x concentration obtained for each group of molecules experiencing a temperature range while flowing through the reactor. The calculated NO_x concentrations as a function of the temperature range are plotted in Fig. 5(b), for a 50% N_2/50% O_2 gas mixture. These results are obtained by the quasi-1D chemical kinetics model, using the plasma conditions (*i.e.*, temperature and power density profiles) which describe each of the distributions and that are obtained from the higher dimensional models, as explained before. The overall NO_x concentration of 3.8% (see Fig. 3(a)) is calculated by weighted average over these ten groups. High values of NO_x concentrations are obtained for gas molecules experiencing a temperature between 2600 K and 3500 K. This is beneficial because as indicated in Fig. 5(a), more than 60% of the gas molecules experience a temperature between 2600 and 3000 K along their journey through the reactor. The reason for this highest NO_x production is that the trajectories of these gas molecules are located in the hottest region of the arc (see ESI, Fig. S4, section S.16†). Consequently, these gas molecules experience a higher temperature and a higher power, so that more reactive species are produced, resulting in a higher NO_x concentration.

Mode II. When the arc operates in the steady arc mode, two main factors are responsible for the record-high NO_x concentrations achieved, as revealed by our combined models. First, a stable arc is located in the centre of the reactor, able to treat all the gas molecules that flow through the reactor. This is in stark contrast to the gas fraction passing through the arc plasma in other types of GA reactors, as mentioned above. As can be seen in Fig. 6(a), the hot plasma zone of the steady arc mode covers a large portion of the reactor. The second reason for the high NO_x concentration is the distinct plasma chemistry occurring in the steady arc mode, compared to the rotating arc mode. While the rotating arc treats the gas multiple times for a short period of time (about 4 ms), the steady arc treats the gas only once for a prolonged duration (up to 10 ms), heating the gas up to 2600 K until it leaves the reactor. At this high gas temperature in the steady arc, VT relaxations occur at a very high rate, and the gas and vibrational temperature reach thermal equilibrium. Indeed, Fig. 6(b) clearly demonstrates that both the gas translational and vibrational temperatures are constant around 2600 K, unlike the temperature profile of the rotating arc in Fig. 4(b), where this VT equilibrium is only reached for less than 4 ms. In this thermal equilibrium state, the vibrationally-promoted Zeldovich mechanism is still the most important reaction pathway for NO_x formation. This pathway produces even more NO_x than in the rotating Mode I, since the constant vibrational temperature of 2600 K is higher than the average vibrational temperature achieved in the rotating mode. However, since the gas temperature is also at 2600 K, the thermal Zeldovich mechanism of ground state N_2 is also significant. Overall, our model predicts that the vibrationally-promoted Zeldovich mechanism is responsible for 70% of the formed NO_x, compared to the 99% of the rotating arc of Mode I. The extra contribution from the thermal (ground state) pathway in this thermal equilibrium state, in combination with the 100% gas fraction passing through the arc, explains the higher NO_x production in this steady arc mode.

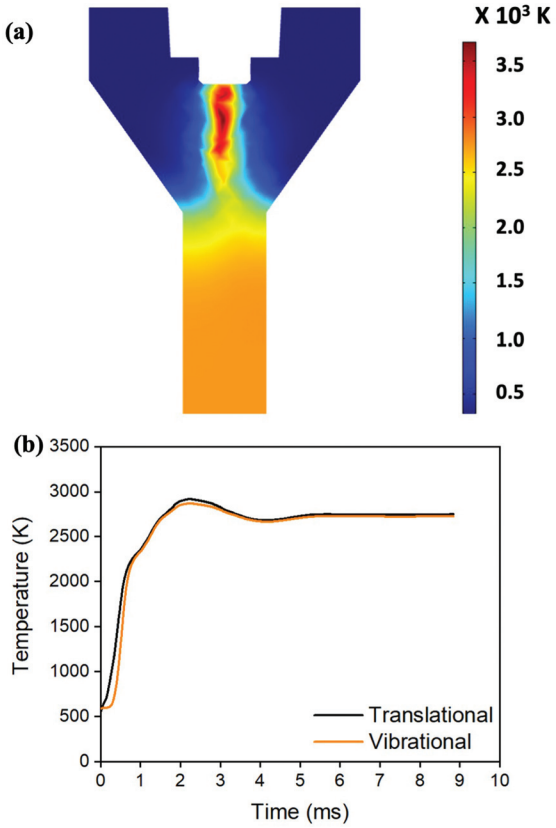

Fig. 6 Calculated plasma gas temperature for an arc in Mode II (a) and the time evolution of the translational and vibrational temperature of the N_2 molecules (b).

Conclusions

We present here highly efficient NO_x production in a novel atmospheric-pressure RGA reactor.

The reactor can be operated in two distinct plasma arc modes: (i) a rotating arc with variable length (Mode I), which is the typical mode in the RGA reactor, and (ii) a steady arc with stable length (Mode II), that could only be achieved at

supplied power above 180 W. We measured the NO_x concentrations for different gas feed ratios, exploring the performance of both modes. When the arc is in Mode I, we obtained NO_x concentrations up to 3.4%, at an energy cost of 2.4 MJ mol^{-1}, which are generally better than the results obtained up to now in atmospheric pressure plasma reactors. However, when the arc is in steady mode (Mode II), even higher NO_x concentrations are achieved, up to 5.5%, *i.e.*, 1.7 times higher than the maximum concentration obtained by the rotating arc mode, with an energy consumption of 2.5 MJ mol^{-1} (or *ca.* 50 kW h kN^{-1}). To our knowledge, these are by far the highest NO_x concentrations that have so far been achieved in an atmospheric pressure plasma reactor.

To gain deeper insight into the behaviour of the arc and the processes taking place in both modes, we performed a combination of five different types of modelling, *i.e.*, gas flow, 3D thermal and 2D non-thermal plasma modelling, particle tracing simulations, as well as quasi-1D chemical kinetics modelling. This innovative, combined modelling study can provide a detailed description of the plasma arc, as well as of the behaviour of gas molecules and chemistry inside the reactor.

Our modelling results reveal that the highest NO_x concentration achieved in the steady arc mode is because the hot plasma zone covers a large portion of the reactor body, permitting all gas molecules to be treated while flowing through the reactor and for a prolonged duration. This is in stark contrast with other GA reactors described in literature, where typically only about 15% of the gas passes through the actual arc,[15,16] thus explaining the much higher NO_x concentrations achieved in our case. Another reason is that both the gas and vibrational temperatures are in equilibrium at around 2600 K, permitting NO_x formation to occur through both the vibrationally-promoted and the thermal Zeldovich mechanisms.

On the other hand, for NO_x formation in the rotating arc mode, our models illustrate that the majority of the gas molecules experience a temperature range between 2600 and 3000 K which is a hot region in the plasma arc. The main NO_x formation pathway here is the vibrationally-promoted Zeldovich mechanism, because of the non-equilibrium between gas and vibrational temperatures when the gas does not pass through the arc, due to the very fast gas cooling which inhibits the relaxation of the vibrationally excited molecules.

The generation of "fixed" or "reactive" nitrogen in high concentrations using air plasma is very promising for sustainable agriculture. As plasma is electricity-driven, and can easily be switched on/off, it is very suitable for coupling with fluctuating renewable electricity, for peak shaving and grid stabilization, and small-scale decentralized fertilizer production. The promising results obtained in the RGA on a small scale are encouraging for further research to be performed on reactor upscaling. Different factors must be thoroughly studied when scaling the flow rate, input power and reactor geometry to industry requirements. Questions arise whether the transition of the arc from a non-thermal towards a more thermal plasma would occur, and whether quenching becomes critical to avoid the loss of NO_x into N_2 and O_2 through the back-reactions of the Zeldovich mechanism. In addition, the question of optimum quenching and mitigation of excessive heat loss to the surroundings by active heat recovery would have to be answered. Moreover, the use of pulsed power sources should also be investigated, because short pulses (*e.g.*, nanosecond duration) may direct a higher fraction of the energy input towards vibrational excitation *via* electron activation, while simultaneously keeping gas heating to a minimum. Finally, careful and systematic tuning of the reactor geometry through vigorous experimental testing is also very important.

Conflicts of interest

There are no conflicts to declare.

Acknowledgements

This research was supported by a Bilateral Project with N2 Applied, the Excellence of Science FWO-FNRS project (FWO grant ID GoF9618n, EOS ID 30505023) and by the European Research Council (ERC) under the European Union's Horizon 2020 research and innovation programme (grant agreement no 810182 – SCOPE ERC Synergy project). The calculations were performed using the Turing HPC infrastructure at the CalcUA core facility of the Universiteit Antwerpen (UAntwerpen), a division of the Flemish Supercomputer Center VSC, funded by the Hercules Foundation, the Flemish Government (department EWI) and the UAntwerpen. We also thank J.-L. Liu for the RGA design, L. Van 't dack and K. Leyssens for MS calibration and practical support, and K. Van 't Veer for the fruitful discussions on plasma kinetic modelling and for calculating the electron energy losses.

Notes and references

1 V. Smil, *Nature*, 2004, **431**, 909–911.
2 D. B. Graves, L. B. Bakken, M. B. Jensen and R. Ingels, *Plasma Chem. Plasma Process.*, 2019, **39**, 1–19.
3 J. G. Chen, R. M. Crooks, L. C. Seefeldt, K. L. Bren, R. M. Bullock, M. Y. Darensbourg, P. L. Holland, B. Hoffman, M. J. Janik, A. K. Jones, M. G. Kanatzidis, P. King, K. M. Lancaster, S. V. Lymar, P. Pfromm, W. F. Schneider and R. R. Schrock, *Science*, 2018, **360**, eaar6611.
4 V. Smil, *Energy in nature and society General energetics of complex systems*, The MIT Press, 2008.
5 N. Cherkasov, A. O. Ibhadon and P. Fitzpatrick, *Chem. Eng. Process. Process Intensif.*, 2015, **90**, 24–33.
6 C. J. Dawson and J. Hilton, *Food Policy*, 2011, **36**, S14–S22.
7 A. Bogaerts and E. C. Neyts, *ACS Energy Lett.*, 2018, 3.
8 R. Ingels and D. B. Graves, *Plasma Med.*, 2015, **5**, 257–270.
9 R. Snoeckx and A. Bogaerts, *Chem. Soc. Rev.*, 2017, **46**, 5805–5863.

10 R. Snoeckx, S. Heijkers, K. Van Wesenbeeck, S. Lenaerts and A. Bogaerts, *Energy Environ. Sci.*, 2016, **9**, 999–1011.
11 K. Birkeland, *Trans. Faraday Soc.*, 1906, **2**, 98–116.
12 S. Eyde, *J. Ind. Eng. Chem.*, 1912, **4**, 771–774.
13 W. S. Partridge, R. B. Parlin and B. J. Zwolinski, *Ind. Eng. Chem.*, 1954, **46**, 1468–1471.
14 M. Rahman and V. Cooray, *Opt. Laser Technol.*, 2003, **35**, 543–546.
15 W. Wang, B. Patil, S. Heijkers, V. Hessel and A. Bogaerts, *ChemSusChem*, 2017, **10**, 2110.
16 E. Vervloessem, M. Aghaei, J. F. N. Hafezkhiabani and A. Bogaerts, *ACS Sustainable Chem. Eng.*, 2020, **8**, 9711–9720.
17 T. Kim, S. Song, J. Kim and R. Iwasaki, *Jpn. J. Appl. Phys.*, 2010, **49**, 126201.
18 B. Mutel, O. Dessaux and P. Goudmand, *Rev. Phys. Appl.*, 1984, **19**, 461–464.
19 R. I. Asisov, V. K. Givotov, V. D. Rusanov and A. Fridman, *Sov. Phys., High Energy Chem.*, 1980, **14**, 366.
20 B. S. Patil, N. Cherkasov, J. Lang, A. O. Ibhadon, V. Hessel and Q. Wang, *Appl. Catal., B*, 2016, **194**, 123–133.
21 R. D. Hill, I. Rahmim and R. G. Rinker, *Ind. Eng. Chem. Res.*, 1988, **27**, 1264–1269.
22 W. Bian, X. Song, J. Shi and X. Yin, *J. Electrostat.*, 2012, **70**, 317–326.
23 N. Rehbein and V. Cooray, *J. Electrostat.*, 2001, **51–52**, 333–339.
24 W. L. Chameides, D. H. Stedman, R. R. Dickerson, D. W. Rusch and R. J. Cicerone, *J. Atmos. Sci.*, 1977, 143–149.
25 X. Pei, D. Gidon, Y. J. Yang, Z. Xiong and D. B. Graves, *Chem. Eng. J.*, 2019, **362**, 217–228.
26 X. Pei, D. Gidon and D. B. Graves, *J. Phys. D: Appl. Phys.*, 2020, **53**, 044002.
27 J. F. Coudert, J. M. Baronnet, J. Rakowitz and P. Fauchais, in Proc. 3rd Int. Symp. on Plasma Chemistry, 1977.
28 B. S. Patil, F. J. J. Peeters, G. J. van Rooij, J. A. Medrano, F. Gallucci, J. Lang, Q. Wang and V. Hessel, *AIChE J.*, 2018, **64**, 526–537.
29 S. Van Alphen, F. Jardali, J. Creel, G. Trenchev, R. Snyders and A. Bogaerts, *Sustainable Energy Fuels*, 2021, Submitted.
30 COMSOL Multiphysics.
31 M. Ramakers, G. Trenchev, S. Heijkers, W. Wang and A. Bogaerts, *ChemSusChem*, 2017, **10**, 2642–2652.
32 E. Cleiren, S. Heijkers, M. Ramakers and A. Bogaerts, *ChemSusChem*, 2017, **10**, 4025–4036.
33 G. Trenchev, S. Kolev, W. Wang, M. Ramakers and A. Bogaerts, *J. Phys. Chem. C*, 2017, **121**, 24470–24479.
34 G. Trenchev, S. Kolev and A. Bogaerts, *Plasma Sources Sci. Technol.*, 2016, **25**, 035014.
35 S. Kolev, S. Sun, G. Trenchev, W. Wang, H. Wang and A. Bogaerts, *Plasma Processes Polym.*, 2017, **14**, 1600110.
36 S. Pancheshnyi, B. Erismann, G. J. M. Hagelaar and L. C. Pitchford, Computer code ZDPlasKin.